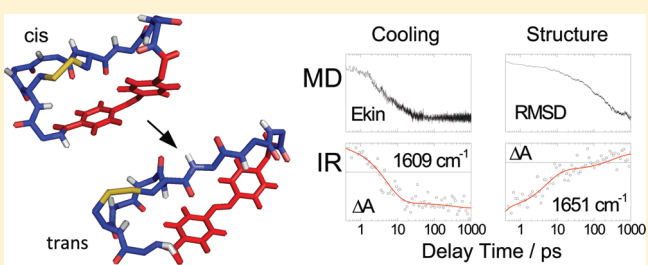


Real Time Observation of Ultrafast Peptide Conformational Dynamics: Molecular Dynamics Simulation vs Infrared Experiment

Phuong H. Nguyen,[†] Heike Staudt,[‡] Josef Wachtveitl,[‡] and Gerhard Stock*,[§][†]Laboratoire de Biochimie Theorique - UPR 9080, Institut de Biologie Physico-Chimique, 13, rue Pierre et Marie Curie, F-75005 Paris, France[‡]Institute of Physical and Theoretical Chemistry, Goethe University, 60438 Frankfurt, Germany[§]Biomolecular Dynamics, Institute of Physics, Albert Ludwigs University, 79104 Freiburg, Germany

Supporting Information

ABSTRACT: Employing nonequilibrium molecular dynamics (MD) simulations and transient infrared (IR) spectroscopy, a joint theoretical/experimental study on a water-soluble photo-switchable octapeptide designed by Renner et al. [*Biopolymers* 2002, 63, 382] is presented. The simulations predict the cooling of the hot photoproducts on a time scale of 7 ps and complex conformational rearrangements ranging from a few picoseconds to several nanoseconds. The experiments yield a dominant fast relaxation time of 5 ps, which is identified as the cooling time of the peptide in water and also accounts for initial conformational changes of the system. Moreover, a weaker component of 300 ps is found, which reflects the overall conformational relaxation of the system. The virtues and the limitations of the joint MD/IR approach to describe biomolecular conformational rearrangements are discussed.



1. INTRODUCTION

Recent experiments and simulations have shown that conformational dynamics is ubiquitous in biomolecules and may thus be important for their functionality.^{1,2} This is not only true for large-scale molecular rearrangements as in folding and aggregation but also holds for small amplitude local transitions which are often important in molecular recognition. For example, the binding mechanism of conformational capture requires that several thermally populated conformational states are available.³ Differing often only in some coordinates of a few peptide residues, these metastable states can be observed in classical molecular dynamics (MD) simulations and are also increasingly seen in experiment.^{4,5} So far, however, only little is known about the time scales of these processes. Depending sensitively on barrier heights (which are difficult to parametrize), calculated transition rates are known to heavily reflect the employed MD force field. Hence, even for simple systems such as small polyalanines, it is largely unclear whether possible transitions between the extended (β and polyproline II) and helical (α and 3_{10}) regions of the Ramachandran plot occur on, say, 10 ps or 10 ns.⁶ In fact, surprisingly little is known about the time scale of the elementary steps of biomolecular dynamics.

Following the initial photoexcitation into a nonstationary conformational state, transient infrared (IR) spectroscopy represents a powerful experimental approach to the real-time observation of structural dynamics.^{7–11} The preparation of the system can be achieved, for example, by inserting a

photoswitchable molecule into the side chains¹² or the backbone^{13,14} of a biopolymer. A particularly rapid conformational rearrangement was observed for the octapeptide fragment H-Ala-Cys-Ala-Thr-Cys-Asp-Gly-Phe-OH, which was connected head to tail via (4-aminomethyl)-phenylazobenzoic acid as well as by a disulfide bridge.^{15–17} Transient visible (vis) pump and IR probe experiments on this bicyclic azobenzene peptide (bcAMPB) suggested that the main conformational changes of the peptide following *cis* → *trans* photoisomerization are completed within only 20 ps.¹⁶ Transient two-dimensional IR spectroscopy,¹⁷ on the other hand, showed substantial changes of the spectra for times up to 1 ns. Optical pump probe spectroscopy¹⁸ yielded two kinetic components with time constants of 100 and 1000 ps. Accompanying nonequilibrium MD simulations of bcAMPB revealed fast conformation dynamics on a 50–100 ps time scale followed by 500–1000 ps conformational equilibration.^{19,20} Due to the uncertainties in the interpretation of the experiments and of the validity of the computational methods, the correct mechanism and the dynamical evolution of the photoinduced conformational rearrangement are not yet resolved in detail.

Another issue of interest represents the role of the solvent which may significantly affect biomolecular dynamics. A well-established effect of the solvent is the cooling of the hot

Received: August 18, 2011

Revised: September 16, 2011

Published: September 22, 2011

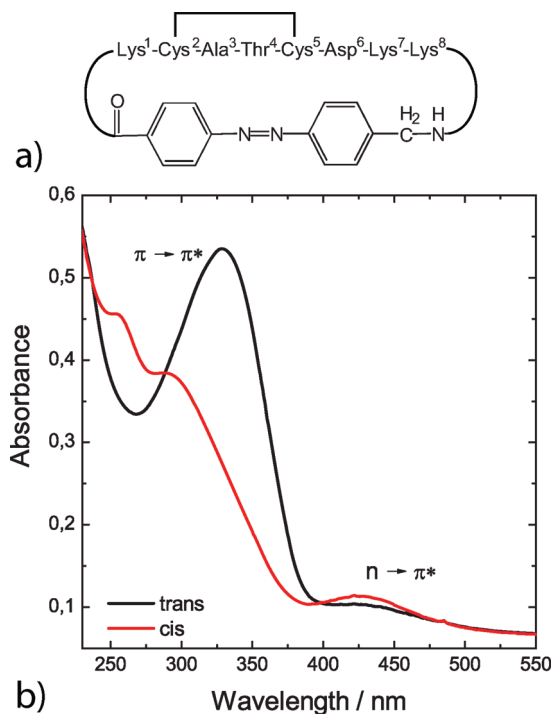


Figure 1. (a) Structure and amino acid labeling of the water-soluble bicyclic azobenzene peptide bcAMPBw. (b) Stationary UV-vis spectrum of the *cis* and the *trans* isomer of bcAMPBw in D_2O .

photoproduct,^{21–28} which is reflected by the disappearance of a red-shifted hot band of the amide I band.^{29,30} The studies on bcAMPB were performed in dimethylsulfoxide (DMSO), which resulted in cooling times of 4 and 5 ps in the IR and optical experiments, respectively. Yet it is unclear if or to what extent the solvent also affects the conformational dynamics of bcAMPB. New evidence may be obtained from a water-soluble version of the photoswitchable peptide, henceforth termed bcAMPBw, which was obtained by Moroder and co-workers³¹ through the introduction of charged side chains (see Figure 1a). So far, only an optical pump probe study on bcAMPBw was presented,³² which reported time scales of 3 ps (presumably reflecting cooling) and 50 ps (presumably reflecting conformational dynamics), which are about a factor of 2 faster than the time scales reported for bcAMPB in DMSO.

To learn about the effects of the solvent on the photoinduced dynamics and to shed some light on the ultrafast conformational dynamics of photoswitchable peptide in general, in this work we perform a joint theoretical/experimental study on the water-soluble photoswitchable peptide bcAMPBw. Following the historical course of our investigations, we first present our equilibrium simulations of bcAMPBw, which are shown to agree well with existing nuclear magnetic resonance (NMR) experiments.³¹ Employing a previously introduced methodology,^{19,20} we then perform nonequilibrium MD simulations of the photoinduced dynamics, which yield a cooling time of 7 ps and complex conformational relaxation dynamics ranging from picoseconds to nanoseconds. Subsequently performed transient vis/IR experiments on bcAMPBw yield two time scales of interest: a dominant fast relaxation of 5 ps, which mainly accounts for the cooling time of the peptide in water, and a weaker component of 300 ps, which reflects the conformational relaxation of the system.

II. METHODS

A. MD Simulations. All simulations were performed with the GROMACS program suite,³³ using the GROMOS96 united atom force field 43a1³⁴ to model the bcAMPBw peptide and the simple-point-charge (SPC) model of ref 35 to describe the water solvent. Initial structures of the bcAMPBw molecule were obtained from NMR experiments³¹ and placed in an octahedral box containing ≈ 1500 water molecules. Two chloride ions were added to neutralize the system. Covalent bonds containing hydrogen atoms were constrained by the procedure SHAKE³⁶ with a relative geometric tolerance of 0.0001. The particle-mesh Ewald method was employed to treat the long-range electrostatic interactions.³⁷ The nonbonded interaction pair list was updated every 5 fs, using a cutoff of 1.4 nm.

The *equilibrium* simulations of the *cis* and the *trans* isomer of bcAMPBw were carried out by using the replica-exchange module implemented in GROMACS, and the details were given in ref 38. In brief, starting from the solvated systems described above, standard NPT simulations were performed at $T = 300$ K and constant pressure (1 atm) for 100 ps, using the Berendsen coupling method.³⁹ The systems were then equilibrated further at constant temperature (300 K) and constant volume for another 100 ps. The final structure of this simulation was employed as the starting structure for all 40 replicas, which covered a temperature range from 280 to 500 K. First, each replica was run independently at its own temperature for 200 ps. Then the exchange procedure between the replicas was turned on, using a time step of 2 ps between two attempts of exchange. Each replica was run for 15 ns, yielding a total sampling time of 1200 ns for the *cis* and the *trans* isomers of bcAMPBw. The data were collected every 0.1 ps.

All *nonequilibrium* simulations were carried out using the MD methodology detailed in refs 19 and 20. In brief, 400 statistically independent initial conformations were selected from the 15 ns equilibrium trajectory of *cis* bcAMPBw. To account for the *cis* \rightarrow *trans* photoisomerization process, we employed a minimal model for the corresponding potential-energy surfaces that diabatically connects the excited-state S_1 of the *cis* isomer with the ground state S_0 of the *trans* isomer (see Figure 1 of ref 19). The photoexcitation of the system by an ultrashort laser pulse was mimicked by instantly switching from the ground-state N=N torsional potential S_0 to the excited-state potential S_1 . Following this nonequilibrium preparation at time $t = 0$, the system isomerizes along the diabatic N=N torsional potential within ≈ 0.2 ps. After isomerization (i.e., for times ≥ 500 fs), the N=N torsional potential is switched back to its ground state form, and a standard MD simulation was performed up to 1 ns. For the first 50 ps, each trajectory was simulated at constant total energy (NVE) using a time step of 0.2 fs. Subsequently, the MD simulations were performed at a constant temperature of 300 K (NVT) with a time step of 2 fs, using the Berendsen method³⁹ with a temperature coupling constant of 0.1 ps. Following the nonequilibrium simulations, the time-dependent observables of interest were obtained via an ensemble average over the initial distribution.

B. Spectroscopy. The water-soluble azopeptide bcAMPBw was prepared as described in ref 31. Fourier transform infrared (FTIR) spectra were obtained with a Vector 22 spectrometer (Bruker). To this end, the sample was dissolved in D_2O (99.9%) and concentrated to an optical density of ≈ 0.5 at 330 nm in a CaF_2 cuvette with $10\ \mu m$ optical path length. The same cuvette

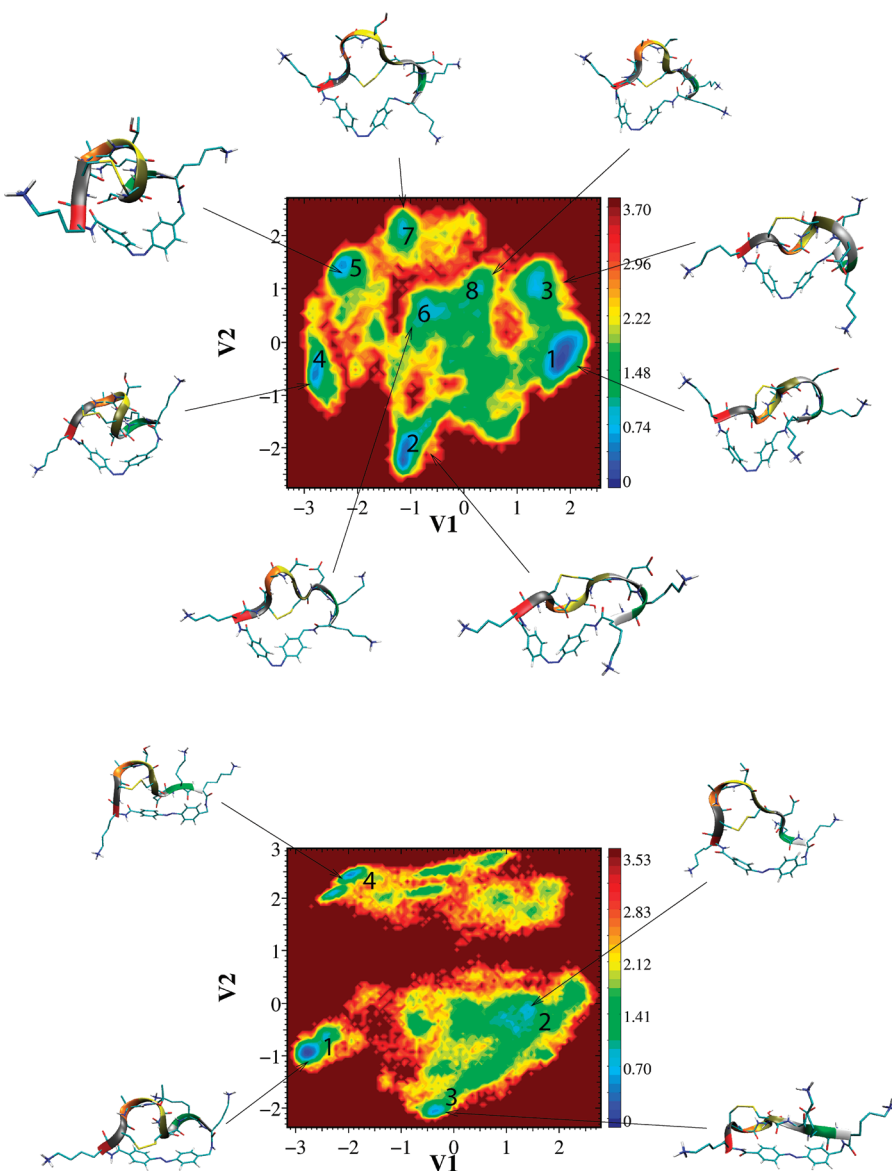


Figure 2. Free energy landscapes (in kcal/mol) of the *cis* (top) and *trans* (bottom) isomers of bcAMPBw in water, plotted as a function of the first two principal components.

was also used for cw UV/vis spectroscopy using a Specord S100 (Analytic Jena). At thermal equilibrium and room temperature, the azopeptide is in its *trans* conformation.³² To accumulate *cis* azopeptide, the sample was illuminated with the light of a Hg–Xe lamp (Hamamatsu) that passed UG1 and WG320 glass filters (Schott). This results in light with a central wavelength of 365 nm, which was employed to excite the $\pi \rightarrow \pi^*$ band of azobenzene. This way, about 70–80% of the *cis* form can be formed in the photostationary state. A filter combination of BG3 and GG420 (central wavelength 435 nm) was used to excite the $n \rightarrow \pi^*$ transition to reaccumulate the *trans* azopeptide, resulting in >90% of the *trans* form in the photostationary state.

The experimental setup for vis pump/IR probe spectroscopy was described in detail elsewhere.⁴⁰ In brief, pulses from a femtosecond amplified laser system (Clark CPA 2001, 1 kHz repetition rate) were converted to pump pulses $\lambda_p = 425$ nm with 460 nJ to excite the $n \rightarrow \pi^*$ transition of the *cis* form and examine the *cis* \rightarrow *trans* direction by using a noncollinear optical parametric

amplifier and subsequent sum frequency mixing with a 775 nm pulse in a β -BBO crystal ($d = 0.1$ mm, $\theta = 26^\circ$). The IR probe pulses were generated by a two-stage collinear optical parametric amplifier and subsequent difference frequency mixing of signal and idler. The polarizations of pump and probe pulses were oriented in a magic angle (54.7°) to avoid orientation contributions to the transient data. Spatial and temporal overlap of pump and probe pulses in the sample was adjusted using a ZnSe substrate. The spectral resolution of the experiment was 11.3 nm, and the temporal cross-phase modulation was ≈ 0.25 ps. Between –2 and 1 ps the step width between individual measurement points was 100 fs. For longer delay times, 70 exponential steps were taken to a maximum delay time of 1.8 ns. The used CaF_2 cuvette had an optical path length of 50 μm , resulting in an optical density of 2.5 at 330 nm. The cuvette with a volume of about 25 μL was moved laterally and rotated at the same time to ensure shot to shot exchange of the sample.

During the transient measurements, the sample was constantly exposed to light with a wavelength centered at 365 nm (see above) to accumulate the *cis* form of the azopeptide. From the steady state experiments, it can be estimated that the sample reaches the photostationary state after a few minutes. UV/vis absorption spectra were taken before and after the time-resolved experiments to verify constant isomer ratios and monitor the accumulation of photodegradation products. After a few hours of measurement, degradation of the azobenzene switch can be observed in the control UV/vis spectra, but averages of the first 20 scans and the last 20 scans of the transient measurements do only show differences in their signal amplitude. We therefore suppose that the degradation products do not have an effect on the transient spectra.

For the quantitative data analysis, a kinetic model was used which describes the data as a sum of exponential decays. A Marquart downhill algorithm optimizes n global time constants τ_i for all wavelengths simultaneously with wavelength-dependent amplitudes $A_i(\lambda)$ for each component. Assuming Gaussian pump and probe pulses with a (1/e) cross-correlation width t_{cc} , the transient absorption spectrum is modeled by

$$\Delta A(t, \lambda) = \sum_{i=1}^n A_i(\lambda) \exp\left(\frac{t^2}{4\tau_i^2} - \frac{t}{\tau_i}\right) \frac{1}{2} \left[1 + \operatorname{erf}\left(\frac{t}{t_{cc}} - \frac{t_{cc}}{2\tau_i}\right) \right] \quad (1)$$

The wavelength-dependent fit amplitudes $A_i(\lambda)$ represent the decay-associated spectra of each component. Note that an infinite time constant represents the time-independent offset of the absorbance change at long times. Since the transient difference spectra show contributions of perturbed free induction decay at negative delay times and cross-phase modulation around time zero, the data analysis was restricted to delay times greater than or equal to 0.4 ps.

III. RESULTS AND DISCUSSION

A. Equilibrium Simulations. To get a first impression of the conformational distribution of bcAMPBw, we performed a principal component analysis of the MD simulations at $T = 300$ K, using the ϕ, ψ dihedral angles of the peptide backbone.^{41,42} Restricting ourselves to the first two principal components V_1 and V_2 , we calculated the free energy $\Delta G \propto -k_B T \ln P(V_1, V_2)$, where $P(V_1, V_2)$ is the probability distribution along these components. Figure 2 shows the resulting free energy landscapes for the *cis* and the *trans* isomer along with representative molecular structures of bcAMPBw. Tables I and II in the Supporting Information characterize the conformation of these structures in terms of their backbone dihedral angles.

Similar to previous findings for the bcAMPB peptide in DMSO,^{15,38} we notice that the *cis* isomer exhibits numerous coexisting conformational states of similar energy. This high structural heterogeneity is due to the considerable steric constraints occurring in the *cis* isomer, which render the molecule an energetically frustrated system. The structure of the *trans* isomer, on the other hand, is clearly better defined. Compared to the *trans* bcAMPB peptide in DMSO with one dominant and one minorly populated conformation,^{15,38} however, bcAMPBw in water nevertheless shows more structural heterogeneity. This might be a consequence of the additional sterical hindrance due to the three long lysine side chains.

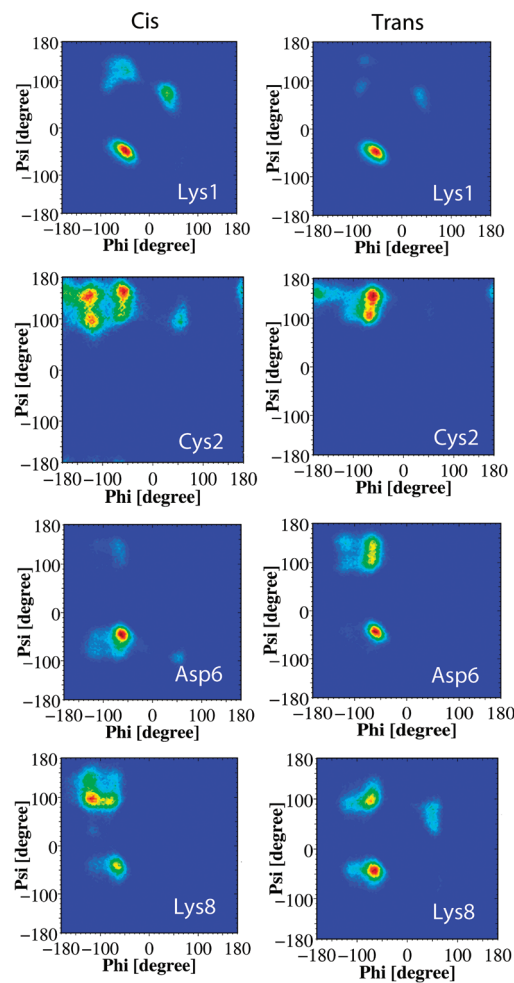


Figure 3. Ramachandran plots of the equilibrium conformational distribution of four selected residues of the *cis* (left) and the *trans* (right) isomer of bcAMPBw.

To characterize the conformational rearrangement upon *cis* → *trans* isomerization in more detail, Figure 3 shows the (ϕ, ψ) probability distributions of four residues of bcAMPBw that show significant structural change, Lys1, Cys2, Asp6, and Lys8. In the *cis* isomer, Lys1 occurs as a mixture of α -helical and β -extended conformations, while (almost) only the α state is left in the *trans* isomer. Cys2 undergoes a transition from a mixed polyproline II/ β state to a polyproline II only state. Hence, the first two residues clearly demonstrate the transition from a heterogeneous to a more homogeneous conformational distribution. While the next three residues (Ala3, Thr4, and Cys5) show only little conformational change, Asp6 is again interesting. It changes from a pure α state to a mixed α /polyproline II state and is thus the only residue whose conformational distribution becomes more complex upon *cis* → *trans* isomerization. Both Lys7 and Lys8 are found in a mixed α -helical/ β -extended conformation. In the case of Lys8 shown in Figure 3, we see that this mixture is shifted to a mostly α -helical conformation.

Our results agree well with the conclusion of Renner et al.³¹ that the *trans* isomer of the peptide exhibits a relatively well-defined structure, while the *cis* isomer consists of an ensemble of similar structures with different backbone geometries. In their NMR study, they reported 32 and 45 interproton distances for

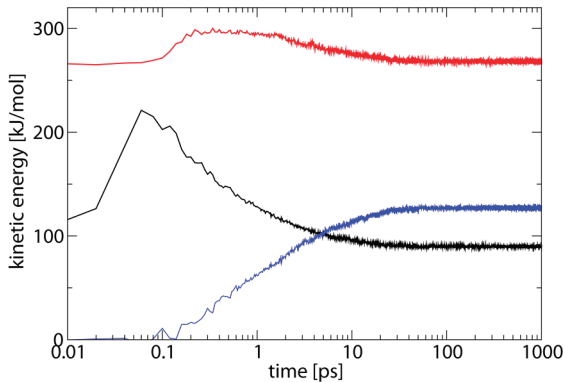


Figure 4. Time evolution of the mean kinetic energy per atom of the azobenzene unit (black), the octapeptide (red), and the water solvent (blue). The latter is defined as $E_S(t) = E_M(0.1 \text{ ps}) - E_M(t)$, where E_M is the kinetic energy of the solvent.

the *cis* and the *trans* isomer of bcAMPBw, respectively, as well as the $^3J(\text{H}^N, \text{H}^\alpha)$ coupling constants of all amino acids. The comparison of experimental and calculated intramolecular distances and 3J couplings in Figure S1 and Tables III–V in the Supporting Information reveals good overall agreement between theory and experiment, although there exist several minor violations. In particular, the calculations satisfy all long-distance constraints, which are most important for the characterization of the peptide conformation.

B. Nonequilibrium Simulations. Having validated the applicability of the MD method to reproduce equilibrium properties of bcAMPBw in water, we now discuss the nonequilibrium dynamics of the peptide following photoisomerization. We focus on two processes which are also observed in transient IR experiments: (i) the vibrational energy transfer from the initially excited photoswitch to the peptide and the subsequent cooling of the molecule in the solvent³⁰ and (ii) the photoinduced conformational change of the system.^{16,17}

Following photoexcitation at time $t = 0$, the excess energy of 320 kJ/mol received by the azobenzene unit is redistributed to the vibrational modes of the peptide and water degrees of freedom. To illustrate this energy transfer process, Figure 4 shows the time evolution of the mean kinetic energy of the azobenzene unit, the octapeptide, and the water solvent. Due to the photoexcitation, the kinetic energy of the photoswitch rises and reaches a peak within 0.1 ps. Accompanying the subsequent decay of the photoswitch energy, the kinetic energies of the peptide and the solvent begin to rise. The vibrational energy propagates through the peptide backbone with a speed of about 0.4 ps per residue.⁴³ At the same time, the peptide loses energy to the solvent, which is reflected in the subsequent decay of the peptide energy, which occurs on a time scale of 7 ps. This value is somewhat larger as the 6 ps cooling time recently found in a nonequilibrium MD study of small peptides in water.²⁸ A possible reason for the deviation might be that an impulsive excitation was assumed in the latter study, while the decay of the photoswitch energy in Figure 4 still delivers energy to the peptide at later times. As a consequence of the cooling of the photoswitch and the peptide, the kinetic energy of the solvent rises on a 3 ps time scale and reaches a plateau after ≈ 20 ps.

There are various observables that can be calculated from the nonequilibrium MD simulations that reflect the photoinduced conformational dynamics of the peptide. To follow up the

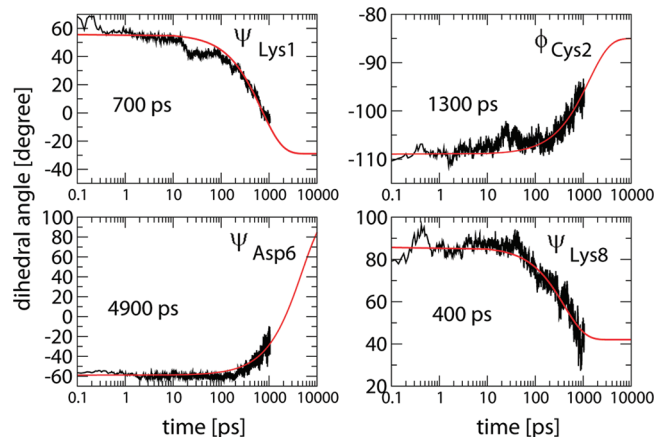


Figure 5. Time evolution and exponential fits of various backbone dihedral angles of bcAMPBw. As the structural transition is not completed within the simulation time of 1 ns, we have included the equilibrium values of the *trans* conformation as long time limits in the fitting procedure and show the fitted time evolution up to 10 ns.

discussion of the conformational rearrangement as shown by the Ramachandran plots of the *cis* and *trans* isomer in Figure 3, we first consider the time evolution of the backbone dihedral angles of the four residues Lys1, Cys2, Asp6, and Lys8. To this end, Figure 5 shows the evolution of the mean value of these observables⁴⁴ when the system changes from *cis* to *trans*. (Figure S2 in the Supporting Information also shows the dynamics of the remaining dihedral angles of bcAMPBw.) As monitored by the ψ dihedral angles, residues Lys1 and Lys8, which are directly connected to the photoswitch, undergo a $\beta \rightarrow \alpha$ transition (see Figure 3). These transitions occur on a time scale of 700 and 400 ps, respectively, and are not completed within the 1 ns of simulation time. To nonetheless obtain reliable exponential fits, we have included the equilibrium values of the *trans* conformation as long time limits in the fitting procedure. Monitored by $\phi_{\text{Cys}2}$, Cys2 undergoes a transition from a mixed polyproline II/ β state to a polyproline II only state on a time scale of 1300 ps. The conformational change of Asp6 from a pure α state to a mixed α /polyproline II state is reflected by an increase of $\psi_{\text{Asp}6}$ with an even longer time constant of 4900 ps. As also found in a site-selective transient IR study of a photoswitchable α helix,⁴⁵ the conformational rearrangement times of various residues may differ considerably. This reveals the complex structural dynamics of the system that cannot be properly described by a single overall time constant.

At variance with the ϕ, ψ backbone dihedral angles, however, the transient IR experiments discussed below do not report on the site-specific dynamics of the peptide but only reveal an averaged response to the conformational dynamics. For the comparison to experiment, it may therefore be instructive to consider some commonly used indicators to monitor *global* conformational change, including (i) the end-to-end distance d_{ee} that connects the two termini of the peptide, (ii) the radius of gyration R_g , and (iii) the root-mean-square deviation (rmsd). Figure 6 shows the time evolution (left) and the probability distribution (right) of these quantities.

The end-to-end distance d_{ee} increases rapidly from 0.6 to 0.8 nm within 0.2 ps, thus reflecting the initial isomerization of the photoswitch. The subsequent time evolution of d_{ee} up to 0.9 nm exhibits a 30 ps and a 2400 ps component. The process is

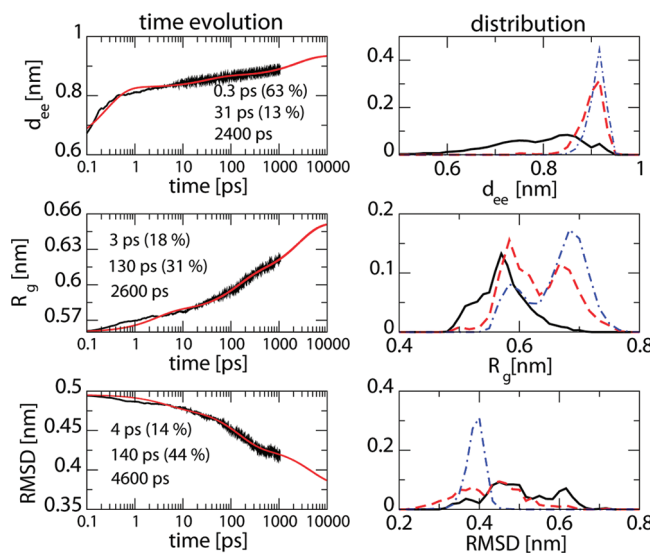


Figure 6. Time evolution (left) and probability distribution (right) of various reaction coordinates that describe the global conformational rearrangement of bcAMPBw following photoexcitation. Shown are (from top to bottom) the peptide end-to-end distance d_{ee} , the radius of gyration R_g , and the root-mean-square deviation (rmsd). The time traces are shown including exponential fits with the three time constants of the fit indicated. The distributions are shown for the first (black lines) and the last (red lines) picosecond of the 1 ns simulation, as well as for the equilibrium *trans* conformation (blue lines).

governed by the competition between the driving force of the photoswitch and the restraining force of the peptide. The distribution of d_{ee} clearly reflects the transition from the disordered *cis* state to the well-defined *trans* state. The radius of gyration $R_g = (\sum_i m_i d_i^2)^{1/2} / (\sum_i m_i)^{1/2}$ is defined as the average of the mass-weighted squared distances of all atoms to the center of mass and is therefore a measure of the overall size of the molecule. As a consequence of the stretching of the peptide backbone, the radius of gyration is found to increase from 0.56 to 0.63 nm within the first nanosecond and is obviously not yet completed. Including the *trans* equilibrium value as the long time limit, we obtain 2600 ps for the slow time scale and 3 ps (18%) and 130 ps (31%) for the two fast components. The rmsd was evaluated for all atoms of the peptide, and the structure of the most prominent *trans* state of bcAMPBw was adopted as the reference geometry. It decays with time constants of 4 (14%), 140 (44%), and 4600 ps, thus reflecting the conformational transition of the peptide from the *cis* to the *trans* form. We note that the distributions of the rmsd at 1 ns exhibit considerable conformational heterogeneity, which only vanishes at long times when the system is in *trans* equilibrium.

It is interesting to note that we need three time scales to represent the time evolution of the global variables in Figure 6, although the time evolution of the individual backbone dihedral angles in Figure 5 was well fitted by a single time constant. The fits of the radius of gyration and the rmsd required three components: a few picoseconds, ≈ 100 ps, and a few nanoseconds. The latter time constant with a weight of $\approx 50\%$ clearly reflects the conformational rearrangement along the peptide backbone. As some dihedral angles also exhibit relatively fast transients [e.g., Thr4 (110 ps) and Lys7 (80 ps), see Figure S2 in the Supporting Information], the weak ($\approx 10\%$) 100 ps component is most likely due to backbone relaxation, too. Of particular

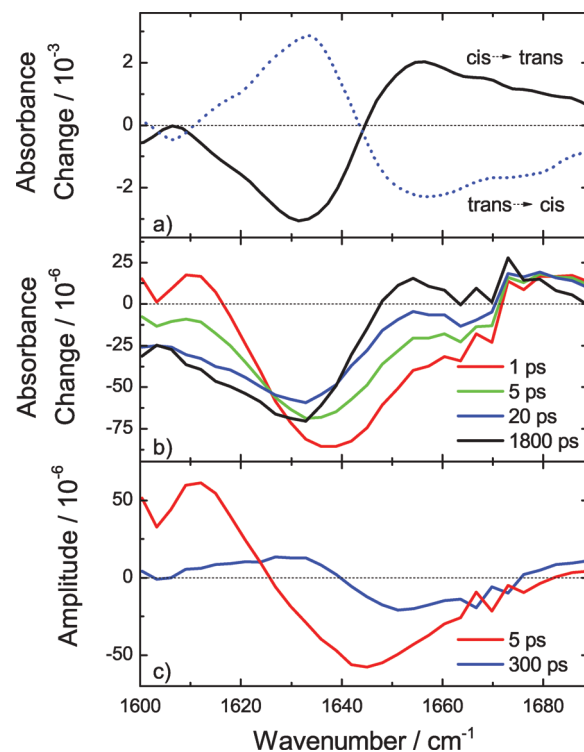


Figure 7. (a) Stationary *cis* \rightarrow *trans* and *trans* \rightarrow *cis* FTIR difference spectra of bcAMPBw in D_2O . (b) Transient *cis* \rightarrow *trans* IR difference spectra at selected delay times and (c) corresponding decay associated spectra obtained from the kinetic model in eq 1.

interest, moreover, is the picosecond time scale because it accounts for an initial fast overall shift of the peptide structure that does not yet affect the backbone dihedral angles. Nonetheless, this initial structural change gives rise to a change of the overall charge distribution of the peptide, which prompts a rapid response of the water solvent (in water typically the response time is of the order of 1 ps⁴⁶). As the measured amide I frequency sensitively depends on the solvent configuration, the initial structural change may lead to a transient frequency shift on a time scale of a few picoseconds.

C. Steady State Spectroscopy. As in the simulation study above, it is instructive to first consider the spectroscopic features of the photoswitchable peptide in equilibrium. To this end, Figure 1b shows the UV/vis spectra of the *cis* and *trans* isomers of bcAMPBw in their photostationary states (see Methods). The absorption bands exhibit the typical spectral signatures of the *cis* and the *trans* form of azobenzene, respectively.⁴⁷ This demonstrates the efficiency of the applied switching process in both directions and ensures the presence of *cis* or *trans* bcAMPBw during the IR experiments, which were performed under the same conditions.

The FTIR spectra of *trans* and *cis* are only marginally shifted ($\approx 2 \text{ cm}^{-1}$) with respect to each other (data not shown). Moreover, the amide I region is overlaid by the spectra of the solvent D_2O , small amounts of HDO, and trifluor acetic acid residual from peptide synthesis.⁴⁸ To eliminate these contributions, we focus on the FTIR *cis* \rightarrow *trans* difference spectrum, obtained by subtracting the IR spectrum of the initial *cis* form from the IR spectrum of the final *trans* form. Hence the resulting spectrum shown in Figure 7a exhibits negative features which

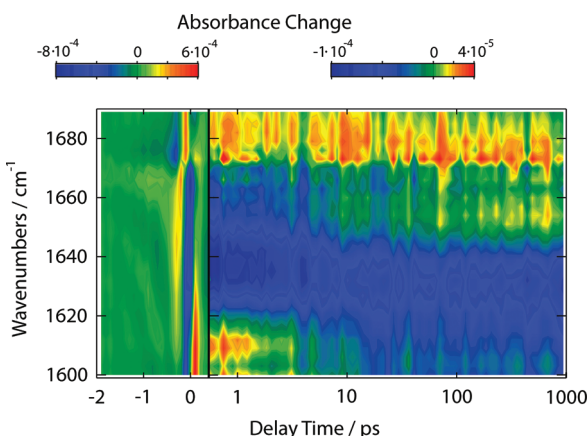


Figure 8. Transient vis pump/IR probe difference spectrum of bcAMPBw in D_2O . The left panel (with a linear time axis from -2 to 0.4 ps) shows the perturbed free induction decay and the cross-phase modulation. The right panel (with a linear time axis from 0.4 to 1 ps and a logarithmic time axis for $t \geq 1$ ps) shows the time evolution of various spectral bands. In particular, the short-lived positive band at 1610 cm^{-1} reflects the cooling of the peptide in the solvent, while the positive absorbance change around 1650 cm^{-1} indicates after $\gtrsim 100$ ps the conformational rearrangement of the peptide.

originate from the initial *cis* conformation and positive features which are due to the generated *trans* form. Also shown is the corresponding *trans* \rightarrow *cis* difference spectrum which mirrors the *cis* \rightarrow *trans* difference spectrum, thus demonstrating the reversibility of the applied photoswitching process.

It is interesting to compare the data for bcAMPBw in D_2O to the results obtained for the related azopeptide bcAMPB in DMSO.¹⁶ First, the absorption band of bcAMPBw is red-shifted by 20 cm^{-1} with respect to the bcAMPB spectrum, which reflects the hydrogen bonding of the peptide to surrounding water molecules. Covering almost 100 cm^{-1} , moreover, the spectrum of bcAMPBw is somewhat broader than its bcAMPB analogue.¹⁶ This effect may also be caused by the interaction with the D_2O solvent, which is known to result in larger line broadening than DMSO. Similar to bcAMPB in DMSO, the pattern of negative and positive difference signals indicates a small ($\approx 2 \text{ cm}^{-1}$) blue shift of the amide I band due to the photoinduced conformational change. The positive difference signal shows a fine structure above 1660 cm^{-1} , which might indicate different spectral position and/or different coupling of the individual amino acids.

D. Transient Spectroscopy. An overview of the transient IR spectrum of bcAMPBw after *cis* \rightarrow *trans* isomerization is shown in Figure 8. At negative delay times (left panel), we observe the typical spectral features of a perturbed free induction decay at 1675 cm^{-1} .⁴⁹ The signals at zero delay time are dominated by cross-phase modulation, which is caused by the media and the pulse parameters and is limited to the cross-correlation width. For delay times larger than 0.4 ps, the right panel shows the time evolution of four spectral bands: (i) a strong positive band around 1680 cm^{-1} that hardly changes with time, (ii) a weaker positive absorbance change centered at 1650 cm^{-1} which becomes visible after ≈ 100 ps, (iii) a broad negative band which undergoes a prominent redshift within ≈ 20 ps, ranging from 1660 cm^{-1} down to almost 1600 cm^{-1} , and (iv) a short-lived positive signal around 1610 cm^{-1} . Alternatively, the spectral evolution can also be observed in cuts of the transient spectrum

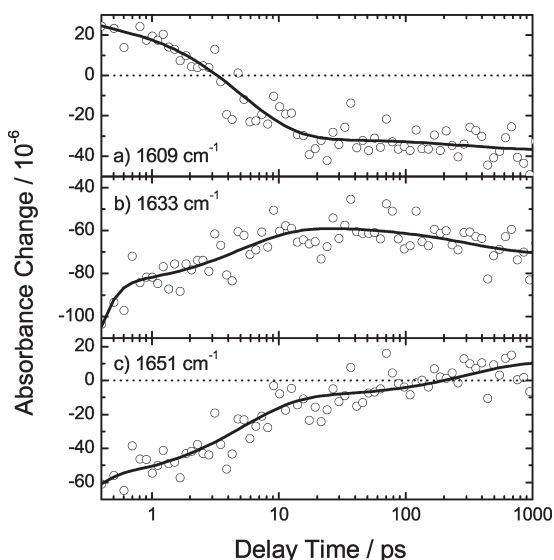


Figure 9. Transient absorbance changes (circles) and results of a global fit analysis (solid lines) at three selected frequencies.

at selected delay times (Figure 7b) and frequencies (Figure 9), respectively.

The prominent positive absorbance change around 1680 cm^{-1} appears very rapidly after photoexcitation. Apart from a slight spectral narrowing at longer times, it hardly changes its position and intensity throughout the entire investigated time range. Nonetheless, the presence of the perturbed free induction decay at this spectral position indicates that this band is due to the chromophore. Together with its characteristic blue shift and subpicosecond appearance, this strongly suggests that the band is caused by the C=O group directly linked to the azobenzene photoswitch (Figure 1).

The most prominent feature of the transient IR spectrum of bcAMPBw is clearly the central negative difference signal, which undergoes a significant red shift on a time scale of 5 ps, which correlates with a blue shift of the amide I band. The same time scale is found for the decay of the positive transient around 1610 cm^{-1} . As demonstrated by Hamm and co-workers,²⁹ the initial observed red shift of the amide I band is due to hot bands. It is caused by the anharmonic coupling of the amide I vibrations to thermally populated low-frequency vibrations of the peptide and therefore monitors the cooling of the photoexcited molecule in the solvent. This finding is in line with the results for bcAMPB, where a time scale of 5 ps was reported for the cooling in DMSO.

It is interesting to note that after ≈ 20 ps the transient IR spectrum (Figure 7b) already resembles to some extent the steady state difference spectrum (Figure 7a). Apart from the cooling process, apparently also initial conformational changes of the peptide happen on the 5 ps time scale. Following the rise of the positive absorbance change around 1650 cm^{-1} after ≈ 100 ps, the transient IR spectrum becomes even more similar to the stationary spectrum. Hence, the time scale of a few hundreds of picoseconds of this feature indicates a second, slower phase of the conformational rearrangement due to photoisomerization. We note, however, that even the spectrum at 1.8 ns does not yet match the stationary spectrum completely, which reveals that the system has not reached its equilibrium within this time.

In line with the above discussion, we find that the time- and frequency-resolved data can be well described by a global fit

including four time constants (<0.2 , 5, 300 ps and ∞). The resulting decay-associated spectra defined in eq 1 are displayed in Figure 7c. By construction, the ∞ component is equivalent to the transient spectrum at maximum time (1.8 ns) shown above and is therefore not explicitly shown. The short time constant, on the other hand, clearly reflects processes directly associated with the *cis* \rightarrow *trans* photoisomerization, which is known to occur on this ultrafast time scale.⁵⁰ As discussed above, the 5 ps time constant accounts for the cooling of the photoexcited molecule in the solvent as well as for initial fast conformational changes. Finally, the time constant of 300 ps reflects the ongoing conformational rearrangement of the peptide.

Showing the transient data as well as the results of the global fit analysis, Figure 9 reveals that the spectral time evolution is indeed well described by the above-discussed time constants. The time trace at 1609 cm^{-1} is dominated by the 5 ps time and reflects directly the cooling process of the system. The time trace at 1651 cm^{-1} nicely accounts for the conformational rearrangement of the peptide, exhibiting contributions from both the 5 and the 300 ps time constant. At 1633 cm^{-1} , in the center of the negative main difference band, the signal even contains contributions from all three time constants of <0.2 , 5, and 300 ps.

IV. DISCUSSION AND CONCLUSIONS

A comparison of the nonequilibrium MD results in Section III B and the above transient IR data of bcAMPB in water reveals a surprisingly good overall agreement of simulation and experiment. To begin, the experimentally identified time scale of *cis* \rightarrow *trans* photoisomerization of <0.2 ps (below the time resolution of the experiment, Figure 8) is naturally found in the calculated rise time of the peptide's kinetic energy (Figure 4) as well as in the initial increase of the end-to-end distance of the peptide (Figure 6). This ultrafast stretching drastically changes the configurational space accessible to the peptide. As the subsequent structural evolution of the peptide is not affected by the dynamics of the photoswitch, bcAMPB represents a versatile model to study the structural rearrangement of a short peptide segment following a conformational transition.

Following the photoexcitation of the system, the cooling of the peptide manifests itself most clearly in the 5 ps decay of the 1610 cm^{-1} band (Figure 9). The process is well reproduced by the simulation through the 7 ps decay of the kinetic energy of the peptide (Figure 4). As discussed in ref 28, the calculated cooling time may decrease by $\approx 25\%$, when a polarizable force field model⁵¹ is used for the water solvent instead of the nonpolarizable SPC model used in this work (see Methods). Hence the neglect of solvent polarizability may explain that the calculated cooling process is somewhat too slow.

The situation is more complex, when we consider the photoinduced conformational changes indicated by the nonequilibrium MD simulations and the transient IR spectra. Again, there appears to be a quantitative agreement concerning the shortest component of 5 ps, which is found in experiment (Figure 9) as well as for the calculated radius of gyration and the rmsd (Figure 6). As discussed above, the initial structural change within 3 and 4 ps monitored by these quantities gives rise to a change of the overall charge distribution of the peptide. This prompts a rapid response of the water solvent (in water typically 1 ps ⁴⁰) which in turn may lead to a transient frequency shift.⁵²

The straightforward one-to-one comparison naturally breaks down when we consider the intermediate time scales of the

conformational dynamics. The 300 ps time seen in experiment (Figure 9) is at least consistent with the intermediate time scale obtained for the global descriptors of conformational change such as the radius of gyration and the rmsd (Figure 6). Accounting for the spectral response of all amide I vibrations of the peptide, however, it cannot be expected that the transient IR spectrum (Figure 8) allows us to disentangle the multitime dynamics of the individual residues (Figure 5). Moreover, a recent study on the calculation of transient IR spectra revealed that the amide I frequency shifts of the individual residues may to some extent cancel each other, thus resulting in quite small frequency shifts and artificially short response times of the overall spectrum.⁵² Together with the limited experimental signal-to-noise ratio at long delay times (Figure 9), this may explain that the significant nanosecond component of the structural rearrangement of the backbone can hardly be seen in experiment. Nonetheless, theory and experiment agree qualitatively at long times in that the conformational rearrangement is not completed on a 1 ns time scale. Taken together, the experimentally found spectral evolution of bcAMPBw in water appears to be a fortunate case, where the spectral bands describing the various dynamical process are—at least to some extent—disentangled and can therefore be readily compared to MD results. Moreover, the overall agreement of experimental and calculated time scales is remarkable in light of the fact that we use a standard biomolecular force field (GROMOS96) which was not parameterized to model dynamical processes.

The situation seems to be more involved in the case of bcAMPB in DMSO, where transient IR experiments suggested that the main photoinduced conformational changes of the peptide are completed within only 20 ps,¹⁶ while accompanying MD simulations found conformational dynamics on several time scales between ≈ 10 and 1000 ps .²⁰ The latter finding is supported by the results of transient two-dimensional spectroscopy,¹⁷ which revealed spectral evolution up to the nanosecond time scale.¹⁷ Furthermore, it is interesting to note that the effects of the solvent appear to be quite small. For example, the measured cooling time is quite similar ($\approx 5\text{ ps}$) in water and DMSO. As the viscosity of D_2O is half of the viscosity of DMSO, it has been suggested that this reduced viscosity is related to the two times faster response obtained in optical experiments.¹⁸ However, the calculated structural rearrangement of the peptide is even somewhat faster for bcAMPB in DMSO than for bcAMPBw in water, possibly caused by the long lysine side chains of the latter.

In conclusion, we have performed a joint MD/IR study of the photoinduced dynamics of a photoswitchable peptide, which allowed us to clearly assign the main time scales found in experiment. The study confirms that transient IR spectroscopy is capable of monitoring the structural evolution of biomolecules. It also shows that isotope labeling and multidimensional techniques may be important to disentangle the complex structural behavior of peptides.

■ ASSOCIATED CONTENT

S Supporting Information. Two tables that characterize the main metastable conformational states of the *cis* and the *trans* isomer of bcAMPBw, a figure and three tables that compare calculated and experimental interproton distances and $^3J(\text{H}^{\text{N}}-\text{H}^{\text{C}})$ couplings for both isomers, and a figure that shows the time evolution of the ϕ, ψ dihedral angles. This material is available free of charge via the Internet at <http://pubs.acs.org>.

■ AUTHOR INFORMATION

Corresponding Author

*E-mail: stock@physik.uni-freiburg.de.

■ ACKNOWLEDGMENT

We thank Christian Renner, Raymond Behrendt, and Luis Moroder for providing the sample of bcAMPBw, Karsten Neumann for significant contributions in setting up the laser system and performing the experiments, and Maja Kobus, Martin Lieder, and Peter Hamm for numerous inspiring and helpful discussions. This work has been supported by the Frankfurt Center for Scientific Computing, the Fonds der Chemischen Industrie, and the Deutsche Forschungsgemeinschaft.

■ REFERENCES

- (1) Henzler-Wildman, K.; Kern, D. *Nature (London)* **2007**, *450*, 964–972.
- (2) Lange, O. F.; Lakomek, N.-A.; Fares, C.; Schröder, G. F.; Walterand, K. F. A.; Becker, S.; Meiler, J.; Grubmüller, H.; Griesinger, C.; de Groot, B. L. *Science* **2008**, *320*, 1471–1475.
- (3) Swain, J. F.; Gerasch, L. M. *Curr. Opin. Struct. Biol.* **2006**, *16*, 102–108.
- (4) Reiner, A.; Henklein, P.; Kieffaber, T. *Proc. Natl. Acad. Sci. U.S.A.* **2010**, *107*, 4955–4960.
- (5) Korzhnev, D. M.; Religa, T. L.; Banachewicz, W.; Ferscht, A. R.; Kay, L. E. *Science* **2010**, *329*, 1312–1316.
- (6) Mu, Y.; Kosov, D. S.; Stock, G. *J. Phys. Chem. B* **2003**, *107*, 5064.
- (7) Hamm, P.; Zanni, M. *Concepts and Methods of 2D Infrared Spectroscopy*; Cambridge University Press: Cambridge, 2011.
- (8) Chung, H.; Khalil, M.; Smith, A. W.; Ganim, Z.; Tokmakoff, A. *Proc. Natl. Acad. Sci. U.S.A.* **2005**, *102*, 612–617.
- (9) Brewer, S.; Song, B.; Raleigh, D.; Dyer, R. *Biochemistry* **2007**, *46* (11), 3279–3285.
- (10) Smith, A. W.; Tokmakoff, A. *Angew. Chem., Int. Ed. Engl.* **2007**, *46*, 7984.
- (11) Hauser, K.; Krejtschi, C.; Huang, R.; Wu, L.; Keiderling, T. A. *J. Am. Chem. Soc.* **2008**, *130*, 2984–2992.
- (12) Kumita, J. R.; Smart, O. S.; Woolley, G. A. *Proc. Natl. Acad. Sci. U.S.A.* **2000**, *97*, 3803.
- (13) Zhao, J.; Wildemann, D.; Jakob, M.; Vargas, C.; Schiene-Fischer, C. *Chem. Commun.* **2003**, *22*, 2810–2811.
- (14) Renner, C.; Moroder, L. *Chem. Bio. Chem.* **2006**, *7*, 869–878.
- (15) Renner, C.; Cramer, J.; Behrendt, R.; Moroder, L. *Biopolymers* **2000**, *54*, 501.
- (16) Bredenbeck, J.; Helbing, J.; Sieg, A.; Schrader, T.; Zinth, W.; Renner, C.; Behrendt, R.; Moroder, L.; Wachtveitl, J.; Hamm, P. *Proc. Natl. Acad. Sci. U.S.A.* **2003**, *100*, 6452.
- (17) Bredenbeck, J.; Helbing, J.; Renner, C.; Moroder, L.; Wachtveitl, J.; Hamm, P. *J. Phys. Chem. B* **2003**, *107*, 8654.
- (18) Wachtveitl, J.; Spörlein, S.; Saltger, H.; Fonrobert, B.; Renner, C.; Behrendt, R.; Oesterhelt, D.; Moroder, L.; Zinth, W. *Biophys. J.* **2004**, *86*, 2350.
- (19) Nguyen, P. H.; Stock, G. *Chem. Phys.* **2006**, *323*, 36–44.
- (20) Nguyen, P. H.; Gorbunov, R. D.; Stock, G. *Biophys. J.* **2006**, *91*, 1224–1234.
- (21) Leitner, D.; Straub, J. *Proteins: Energy, Heat and Signal Flow*; Taylor and Francis/CRC Press: London, 2009.
- (22) Henry, E. R.; Eaton, W. A.; Hochstrasser, R. M. *Proc. Natl. Acad. Sci. U.S.A.* **1986**, *83*, 8982–8986.
- (23) Tesch, M.; Schulten, K. *Chem. Phys. Lett.* **1990**, *169*, 97–102.
- (24) Moritsugu, K.; Miyashita, O.; Kidera, A. *J. Phys. Chem. B* **2003**, *107*, 3309–3317.
- (25) Fujisaki, H.; Straub, J. E. *Proc. Natl. Acad. Sci. U.S.A.* **2005**, *102*, 6726–6731.
- (26) Zhang, Y.; Fujisaki, H.; Straub, J. E. *J. Phys. Chem. B* **2007**, *111* (12), 3243–3250.
- (27) Leitner, D. M. *Annu. Rev. Phys. Chem.* **2008**, *59*, 233–259.
- (28) Park, S. M.; Nguyen, P. H.; Stock, G. *J. Chem. Phys.* **2009**, *131*, 184503.
- (29) Hamm, P.; Ohline, S. M.; Zinth, W. *J. Chem. Phys.* **1997**, *106*, 519–529.
- (30) Botan, V.; Backus, E.; Pfister, R.; Moretto, A.; Crisma, M.; Toniolo, C.; Nguyen, P. H.; Stock, G.; Hamm, P. *Proc. Natl. Acad. Sci. U.S.A.* **2007**, *104*, 12749–12754.
- (31) Renner, C.; Cramer, J.; Behrendt, R.; Moroder, L. *Biopolymers* **2002**, *63*, 382–393.
- (32) Satzger, H.; Root, C.; Renner, C.; Behrendt, R.; Moroder, L.; Wachtveitl, J.; Zinth, W. *Chem. Phys. Lett.* **2004**, *396*, 191–197.
- (33) van der Spoel, D.; Lindahl, E.; Hess, B.; Groenhof, G.; Mark, A. E.; Berendsen, H. J. C. *J. Comput. Chem.* **2005**, *26*, 1701–1718.
- (34) van Gunsteren, W. F.; Billeter, S. R.; Eising, A. A.; Hünenberger, P. H.; Krüger, P.; Mark, A. E.; Scott, W. R. P.; Tironi, I. G. *Biomolecular Simulation: The GROMOS96 Manual and User Guide*; VdfHochschulverlag AG an der ETH Zürich: Zürich, 1996.
- (35) Berendsen, H. J. C.; Postma, J. P. M.; van Gunsteren, W. F.; Hermans, J. In *Intermolecular Forces*; Pullman, B., Ed.; D. Reidel Publishing Company: Dordrecht, 1981; pp 331–342.
- (36) Ryckaert, J. P.; Ciccotti, G.; Berendsen, H. J. C. *J. Comput. Phys.* **1977**, *23*, 327–341.
- (37) Darden, T.; York, D.; Petersen, L. *J. Chem. Phys.* **1993**, *98*, 10089.
- (38) Nguyen, P. H.; Mu, Y.; Stock, G. *Proteins* **2005**, *60*, 485–494.
- (39) Berendsen, H. J. C.; Postma, J. P. M.; van Gunsteren, W. F.; Dinola, A.; Haak, J. R. *J. Chem. Phys.* **1984**, *81*, 3684.
- (40) Neumann, K.; Verhoefen, M.-K.; Weber, I.; Glaubitz, C.; Wachtveitl, J. *Biophys. J.* **2008**, *94*, 4796–4807.
- (41) Mu, Y.; Nguyen, P. H.; Stock, G. *Proteins* **2005**, *58*, 45.
- (42) Altis, A.; Nguyen, P. H.; Hegger, R.; Stock, G. *J. Chem. Phys.* **2007**, *126*, 244111.
- (43) Nguyen, P. H.; Park, S. M.; Stock, G. *J. Chem. Phys.* **2010**, *132*, 025102.
- (44) Since dihedral angles φ represent circular variables, their mean is calculated via $\tan\langle\varphi\rangle = \langle y \rangle / \langle x \rangle = \sum_n \sin \varphi_n / \sum_n \cos \varphi_n$.
- (45) Ihalainen, J. A.; Paoli, B.; Muff, S.; Backus, E. H. G.; Bredenbeck, J.; Woolley, G. A.; Hamm, P. *Proc. Natl. Acad. Sci. U.S.A.* **2008**, *105*, 9588–9593.
- (46) Maroncelli, M.; Fleming, G. R. *J. Chem. Phys.* **1988**, *89* (8), 5044–5069.
- (47) Rau, H. *Angew. Chem., Int. Ed.* **1973**, *12*, 224–235.
- (48) Venyaminov, S. Y.; Prendergast, F. G. *Anal. Biochem.* **1997**, *248*, 234–245.
- (49) Hamm, P. *Chem. Phys.* **1995**, *200*, 415–429.
- (50) Nägele, T.; Hoche, R.; Zinth, W.; Wachtveitl, J. *Chem. Phys. Lett.* **1997**, *272*, 489–495.
- (51) van Maaren, P. J.; van der Spoel, D. *J. Phys. Chem. B* **2001**, *105*, 2618–2626.
- (52) Kobus, M.; Lieder, M.; Nguyen, P. H.; Stock, G. 2011, submitted.